pp. 1–11 (2019)

Spatially resolved modelling of immune responses following a multiscale approach: from computational implementation to quantitative predictions

D. S. Grebennikov*‡‡ and G. A. Bocharov†

Abstract — In this work we formulate a hybrid multiscale model for describing the fundamental immune processes in human immunodeficiency type 1 (HIV) infection. These include (i) the T cell migration in the lymphoid tissue, (ii) the replication cycle of HIV within an infected cell, (iii) the type I interferon (IFN) response of the target cells, and (iv) the spatiotemporal dynamics of the HIV and type I IFN fields. Computational implementation of the hybrid multiscale model is presented. It is based on the use of semi-implicit first-order symplectic Euler method for solving the equations of the second Newton's law for cell migration and the alternating direction method for the initial-boundary value problem for reaction–diffusion equations governing the spatial evolution of the virus and IFN fields in 2D domain representing the lymph node (LN) tissue. Both, the stochastic and deterministic descriptions of the intracellular HIV infection and the IFN reaction are developed. The potential of the calibrated multiscale hybrid model is illustrated by predicting the dynamics of the local HIV infection bursts in LN tissue.

Keywords: Mathematical immunology, multiscale processes, hybrid modelling, HIV infection

MSC 2010: 92-08, 92C17, 92C42

The immune system provides the defense of a host organism against foreign pathogens and tumour development, and plays an active role in tissue and organ regeneration. The modern era of research in immunology is characterized by an unprecedented level of detail about its numerous components functioning together as a whole network-type system [1, 8, 13, 14]. There is a demand for the development of high-resolution detailed mathematical models and their integration into experimental and clinical research to provide a mechanistic tool for the description, analysis and prediction of immune process dynamics under specified conditions.

A multiscale framework in mathematical immunology turned out to be insightful for understanding the pathogenesis mechanisms and identifying potential therapeutic targets for human infections with Mycobacterium tuberculosis [12,18]. Other specific examples of immune system analysis based on multiscale models are the

*Moscow Institute of Physics and Technology (National Research University), Dolgoprudny 141701, Russia. E-mail: dmitry.ew@gmail.com

†Marchuk Institute of Numerical Mathematics, Russian Academy of Sciences, Moscow 119333, Russia. E-mail: gbocharov@gmail.com

‡Sechenov University, Moscow 119991, Russia

This study was supported by the Russian Science Foundation (grant No. 18-11-00171).

studies of early CD8$^+$ T cell immune responses in lymph nodes (LN) [9] and immune processes in LNs [3]. The practical development of a hybrid approach to multiscale modelling of immune processes presents a number of challenges ranging from the numerical accuracy and consistency of the different methods being used to compute the system component dynamics on the one side to the risk of producing modelling artefacts because of system complexity and parameter uncertainty on the other side [5, 6]. In fact, one needs to have clear computational methodologies for the development of various mathematical modelling tools including simple single-level resolution phenomenological models, large-scale multi-compartmental models and high-resolution multiscale models amenable to validation using well-documented infections, e.g., such as human immunodeficiency virus type 1 (HIV) infection.

In Section 1, we present formulation, implementation in 2D and calibration of the mathematical model of cell migration in lymphoid tissue based on the second Newton's law equation. In Section 2, we formulate the reaction–diffusion model of extracellular dynamics of HIV virions and type 1 interferon (IFN) molecules and stochastic model of HIV transmission in LN. In Section 3, the stochastic and deterministic descriptions for the single-level processes, e.g., the intracellular HIV life cycle and type I interferon response induction are formulated and numerically implemented. In Section 4, we explore the hybrid model of the immune response to HIV infection integrating two levels of resolution, i.e., the intracellular regulation of infection and 2D spatial dynamics of cells, viruses and cytokines (IFN) in lymphoid organs.

1. Calibrated model of lymphocyte motility in LN

Immune processes develop in highly organized spatial structures of the lymphoid organs and the lymphatic system. Here we present the model of lymphocyte motility in lymph nodes which was formulated and calibrated in [10]. The equations governing the motion of a system of N cells with coordinates $\mathbf{x}_i$ and radii r_i represent the system of second Newton's law equations:

$$m_i\ddot{\mathbf{x}}_i = \mathbf{F}_i = \sum_{j\neq i}\mathbf{f}_{ij} + \mathbf{f}_i^{\text{mot}} - \mu\dot{\mathbf{x}}_i \quad \text{in } \Omega \subset \mathbb{R}^2, \quad i,j = 1,\ldots,N \tag{1.1}$$

where the right-hand side includes (i) the cell-to-cell interaction force $\mathbf{F}_i^{\text{int}} = \sum_{j\neq i}\mathbf{f}_{ij}$, (ii) the stochastic force of active intrinsic cell motility $\mathbf{f}_i^{\text{mot}}$, and (iii) the dissipative friction force $-\mu\dot{\mathbf{x}}_i$.

The cell-to-cell interaction force $\mathbf{f}_{ij}$ can be adhesive or repulsive depending on the distance h_{ij} from the center of cell i to the membrane of cell j:

$$\mathbf{f}_{ij}(h_{ij}) = \frac{\mathbf{x}_i - \mathbf{x}_j}{h_{ij}} \cdot \begin{cases} -a \cdot f_i^{\text{adh}} \dfrac{L - h_{ij}}{L} + b \cdot f_i^{\text{adh}} \dfrac{(L-h_{ij})^3}{L^3}, & h_{ij} < L \\ 0, & h_{ij} \geqslant L \end{cases}$$

where $h_{ij} = |\mathbf{x}_i - \mathbf{x}_j|$ is the distance between centers of cells, $L = r_i + r_j$ is the sum of i-th and j-th cells radii. Coefficients a and b are set so that the following condition is fulfilled: $f_{ij}(L) = 0, f_{ij}(5L/6) = 0, f_i^{\text{adh}} = \min f_{ij}(x)$, thus leaving the only free parameter f_i^{adh}, which represents the adhesive strength of the contact between cells of certain type, estimated for nonspecific and specific contacts in [10].

The active intrinsic cell motility force $\mathbf{f}_i^{\text{mot}}$ is simulated as stochastic vector sampled by rules of an empirical model of correlated random walk. It implicitly accounts for the effects of T cell interactions with fibroblastic reticular cell network, extracellular matrix fibers and chemokines, all guiding their migration. Every $\Delta t = 30$ s the magnitude and direction of the force are sampled from the certain probability distributions, as described in [10]. After that, the sampled force is corrected to account for contact inhibition of locomotion. The modification consists of shifting the direction of the force vector away from the neighboring cells and decreasing the magnitude of force proportionally to the number of neighboring cells (for details see [10]). The model above was calibrated by experimental data on lymphocyte intranodal imaging and the estimated model parameters are provided in [10].

For numerical integration of the cell motion equations (1.1) the semi-implicit first-order symplectic Euler method with $h_{\text{mot}}^t = 0.02$ min time-step was used:

$$\mathbf{v}_i^{n+1} = \frac{m_i \mathbf{v}_i^n + h_{\text{mot}}^t \cdot \left(\mathbf{F}_i^{\text{int}}(\mathbf{x}_i^n) + \mathbf{f}_i^{\text{mot}}(t^n)\right)}{m_i + h_{\text{mot}}^t \cdot \mu}, \quad \mathbf{x}_i^{n+1} = \mathbf{x}_i^n + h_{\text{mot}}^t \cdot \mathbf{v}_i^{n+1}$$

where $\mathbf{x}_i^n$ and $\mathbf{v}_i^n$ are the coordinate and the velocity of cell i after n steps, respectively, $t^n = t^0 + h_{\text{mot}}^t \cdot n$.

In subsequent multiscale simulations, we consider square computational domain $\Omega = [0, L]^2$, $L = 412$ μm, with periodic boundary conditions for cell movements. We initialize 4489 squarely tiled T cells with $r_i = 3$ μm ($\approx 80\%$ packing density) and run 30 min of simulation time to randomly mix the cells to obtain the initial configuration. Then, one productively infected dendritic cell with $r_{DC} = 6.5$ μm is introduced in the center of the domain.

2. Extracellular dynamics of HIV virions and IFN

2.1. Reaction–diffusion equations for extracellular fields

The dynamics of extracellular fields of free virions $V(\mathbf{x}, t)$ and interferon molecules $I(\mathbf{x}, t)$ are modelled with reaction–diffusion equations ($c = \{V, I\}$):

$$\begin{gathered} \frac{\partial c}{\partial t} = D_c \Delta c + s_c - d_c c \quad \text{in } \Omega_D \\ c(\mathbf{x}, t) = 0 \quad \text{on } \partial\Omega_D, \quad c(\mathbf{x}, 0) = 0 \quad \text{in } \Omega_D \end{gathered} \tag{2.1}$$

where D_c is the diffusion coefficient, d_c is the degradation rate, s_c is a source term describing secretion of the virions or molecules by $N_c(t)$ corresponding cells:

$s_c(\mathbf{x},t) = \sum_{i=1}^{N_c(t)} \rho_c\big|_{\Omega_k}(\mathbf{x})$ (the details of cell-specific production are presented in Section 4), here $|_{\Omega_k}$ denotes the indicator function of the area $\Omega_k = \Omega_k(\mathbf{x}_\mathbf{k}(t)) = \{\mathbf{x} \in \Omega_D : \|\mathbf{x} - \mathbf{x}_\mathbf{k}\| \leqslant r_k\}$ occupied by the kth cell.

The actual boundaries of lymph node are not considered in the model. Instead, we solve (2.1) in the extended domain $\Omega_D = [-l_m, L + l_m]^2$ with zero Dirichlet boundary conditions, where $l_m = 19$ μm is the length of the margins around the domain Ω. This approximation is suitable for the study of local effects of HIV transmission by one infected cell. The boundary value problem (2.1) is solved numerically using alternating direction implicit (ADI) method on a uniform rectangular grid $(x_i, y_j, t_n) = (-l_m + ih^x, -l_m + jh^y, t_0 + nh^t)$, $i, j = 1, \ldots, N_\mathbf{x}$: in the first substep we implicitly discretize x-derivative, in the second — y-derivative,

$$\frac{c_{i,j}^{n+1/2} - c_{i,j}^n}{h^t/2} = \frac{D_c}{(h^x)^2}\delta_x^2 c_{i,j}^{n+1/2} + \frac{D_c}{(h^y)^2}\delta_y^2 c_{i,j}^n + s_c(x_i, y_j, t_n) - d_c c_{i,j}^{n+1/2}$$
$$\frac{c_{i,j}^{n+1} - c_{i,j}^{n+1/2}}{h^t/2} = \frac{D_c}{(h^x)^2}\delta_x^2 c_{i,j}^{n+1/2} + \frac{D_c}{(h^y)^2}\delta_y^2 c_{i,j}^{n+1} + s_c(x_i, y_j, t_n) - d_c c_{i,j}^{n+1}$$

where $\delta_x^2 u_{i,j} = u_{i-1,j} - 2u_{i,j} + u_{i+1,j}$, $\delta_y^2 u_{i,j} = u_{i,j-1} - 2u_{i,j} + u_{i,j+1}$. To obtain $s_c(x_i, y_i, t_n)$ in the grid node $\mathbf{x}^* = (x_i, y_i)$ we use the formula $s_c(\mathbf{x}^*, t_n) = \sum_{k=1}^{N_c(t_n)} \rho_c I_{\Omega_k}(\mathbf{x}^*)(r_k^2 - ||\mathbf{x}^* - \mathbf{x}_\mathbf{k}||^2) \big/ \sum_{\mathbf{x}^* \in \Omega_k}(r_k^2 - ||\mathbf{x}^* - \mathbf{x}_\mathbf{k}||^2)$. The resulting symmetric tridiagonal systems are solved using tridiagonal matrix (Thomas) algorithm for each substep. In numerical simulations, we use $h^x = h^y = 1$ μm, $h^t = 1$min.

2.2. Stochastic model of HIV transmission

The spread of HIV in lymphoid tissues is achieved through two mechanisms: (1) cell-to-cell transmission of viral genomes by infected cells, (2) cell-free infection by extracellular virions secreted by productively infected cells after completion of intracellular replication stages [22]. We consider both mechanisms. The CD4$^+$ T cell can be infected with the rates $\hat{k}_{\text{free}}^{(i)}(t) = k_{\text{free}} \cdot \mathrm{e}^{-(t - t_{\text{inf}}^{(i)})/t_d}$ and $\hat{k}_{\text{cell}}^{(i)}(t) = k_{\text{cell}} \cdot \mathrm{e}^{-(t - t_{\text{inf}}^{(i)})/t_d}$, where $t_{\text{inf}}^{(i)}$ is the moment of beginning of the infection process (i.e., when the cell first came in contact with free virion or infected cell), and $t_d \approx 0.7$ h is characteristic time of decay of infection rates due to downregulation of CD4 molecules expression on the cell membrane [7]. We model these rates proportional to local numbers of free virions and infectious cells (instead of their global concentrations, as defined in [7]):

$$r_{\text{free}}^{(i)} = \hat{k}_{\text{free}}^{(i)}(t) \int_{\Omega_i} V(\mathbf{x}, t)\mathrm{d}\mathbf{x}, \quad r_{\text{cell}}^{(i)} = \hat{k}_{\text{cell}}^{(i)}(t) \cdot N_{\text{neigh}}^{(i)}(t)$$

where $N_{\text{neigh}}^{(i)}$ is the number of infected cells contacting the cell (number of neighbours). We estimate the rates from [22] as $k_{\text{free}} = 1.68 \cdot 10^{-3}$ h^{-1}, $k_{\text{cell}} = 0.76$ h^{-1}.

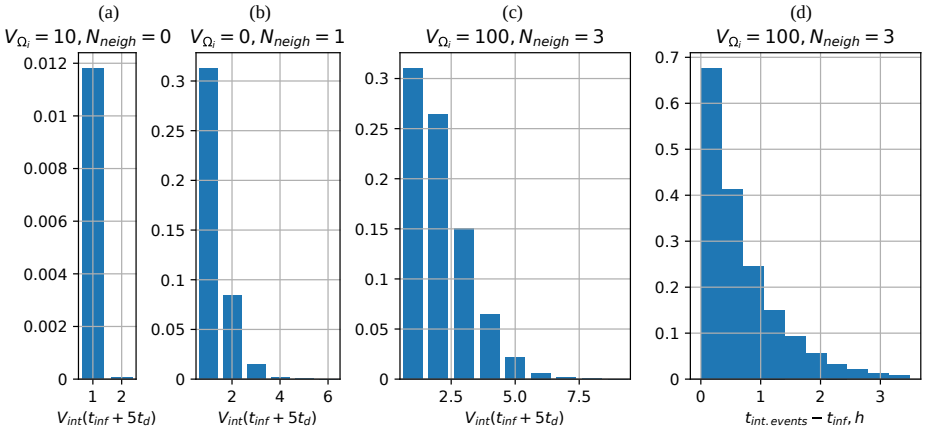

Figure 1. Distributions of integrated proviruses in the infected cell in different infection scenarios (10^5 numerical realizations for each scenario). (a)–(c) Distributions of the numbers of integrated proviruses V_{int} at time $t_{\text{inf}} + 5t_d$. (d) Distribution of the times of provirus integration events since the infection time t_{inf}.

The probability that no new viral genome will be integrated in the nucleus during interval $(t^*, t^* + \tau)$ since the previous integration time t^*, is

$$P(\tau|t^*) = \exp\left(-\int_{t^*}^{t^*+\tau} (k_{\text{free}} V_{\Omega_i}(t) + k_{\text{cell}} N^{(i)}_{\text{neigh}}(t))\, \mathrm{e}^{-(t-t^{(i)}_{\text{inf}})/t_d} \mathrm{d}t\right)$$

where $V_{\Omega_i}(t) = \int_{\Omega_i} V(\mathbf{x}, t)\mathrm{d}\mathbf{x}$. At time $t^{**} = t^* + \tau$, the number of integrated proviruses in cell i will be increased: $V^{(i)}_{\text{int}} = V^{(i)}_{\text{int}} + 1$. This stochastic process is simulated using Temporal Gillespie Algorithm [21], with $V_{\Omega_i}(t)$ and $N^{(i)}_{\text{neigh}}(t)$ being updated every h^t and h^t_{mot} minutes. To reduce computational complexity, the infection events are tracked for each cell from time $t^{(i)}_{\text{inf}}$ till time $t^{(i)}_{\text{inf}} + 5t_d$. The algorithm consists of the following steps. First, we draw a normalized waiting time $\tau' = \mathbb{L}(t^{**}|t^*) = \int_{t^*}^{t^{**}} \Lambda(t)dt$, $\Lambda(t) = (k_{\text{free}} V_{\Omega_i}(t) + k_{\text{cell}} N^{(i)}_{\text{neigh}}(t)) e^{-(t-t^{(i)}_{\text{inf}})/t_d}$, from a standard exponential distribution $\tau' \sim \text{Exp}(1)$. The time t^{**} when a next event will occur is given implicitly by the equation $\mathbb{L}(t^{**}|t^*) = \tau'$. To obtain t^{**} numerically, we approximate $\Lambda(t)$ as constant over time-step h^t_{mot}, assuming $\Delta\Lambda(t) \cdot h^t_{\text{mot}} \ll 1$, where $\Delta\Lambda(t)$ is a change of $\Lambda(t)$ during time-step. For simplicity, let $t^{(i)}_{\text{inf}} = t^0$. At each time-step n, if $\mathbb{L}(t^n|t^0) = h^t_{\text{mot}} \sum_{l=0}^{n-1} \Lambda(t^l) < \tau'$, then algorithm advances to the next time-step. Otherwise, the time of the next event is given by $t^{**} = t^n + (\tau' - \mathbb{L}(t^n|t^0))/\Lambda(t^n)$. Then, $t^* \leftarrow t^{**}$, and the algorithm reiterates by drawing new normalized time τ', and advancing through time-steps until $\mathbb{L}(t^n|t^*) \geqslant \tau'$, when the time of the next event t^{**} is calculated, and so on. Statistical properties of provirus integration events obtained numerically using the described algorithm are illustrated in Fig. 1.

3. Intracellular regulation of HIV infection: combining deterministic and stochastic formulations

In intracellular models presented below, we omit indices $^{(i)}$ for model variables in cell i. We describe the deterministic model of HIV replication and stochastic model of the antiviral IFN response. The deterministic model can be extended to a stochastic model using a hybrid approach proposed in [17], but it is not considered in this paper.

3.1. HIV replication

After HIV provirus is integrated in infected cell, it can remain latent (which is not considered in this model) or become productively infected, in which case the later stages of HIV replication are activated. The model for these replication steps is derived from [11, 15]. It describes the generation of genomic RNA transcripts $V_{g\mathrm{RNA}n}$ and their splicing to V_{dsRNAn}, their export from the nucleus to cytoplasm to become $V_{g\mathrm{RNA}}$ and V_{dsRNA}, and maturation of new virions V_{mat} proportional to $V_{g\mathrm{RNA}}$. The model includes the dynamics of proteins [Tat] and [Rev], which are crucial for regulation of transcription, splicing, and export processes. The deterministic formulation of the model is given by the following ODE system:

$$
\begin{aligned}
\frac{\mathrm{d}V_{g\mathrm{RNA}n}}{\mathrm{d}t} &= [\mathrm{TR}]\cdot V_{\mathrm{int}} - (2k_{sp}(1-\beta f_{\mathrm{Rev}}) + k_{\mathrm{exp}} f_{\mathrm{Rev}} + d_{\mathrm{RNA}})V_{g\mathrm{RNA}n}\\
\frac{\mathrm{d}V_{\mathrm{dsRNAn}}}{\mathrm{d}t} &= k_{sp}(1-\beta f_{\mathrm{Rev}})V_{g\mathrm{RNA}n} - (k_{\mathrm{exp}} + d_{\mathrm{RNA}})V_{\mathrm{dsRNAn}}\\
\frac{\mathrm{d}V_{\mathrm{dsRNA}}}{\mathrm{d}t} &= k_{\mathrm{exp}}V_{\mathrm{dsRNAn}} - (d_{\mathrm{RNA}} + k_{\mathrm{ISG}}\, b_{\mathrm{ISG}})V_{\mathrm{dsRNA}}\\
\frac{\mathrm{d}[\mathrm{Tat}]}{\mathrm{d}t} &= r_{\mathrm{Tat}}V_{\mathrm{dsRNA}} - d_{\mathrm{Tat}}[\mathrm{Tat}], \quad \frac{\mathrm{d}[\mathrm{Rev}]}{\mathrm{d}t} = r_{\mathrm{Rev}}V_{\mathrm{dsRNA}} - d_{\mathrm{Rev}}[\mathrm{Rev}]\\
\frac{\mathrm{d}V_{g\mathrm{RNA}}}{\mathrm{d}t} &= k_{\mathrm{exp}}\, f_{\mathrm{Rev}}\, V_{g\mathrm{RNA}n} - (2\cdot k_{\mathrm{mat}} + d_{\mathrm{RNA}} + k_{\mathrm{ISG}}\cdot b_{\mathrm{ISG}})V_{g\mathrm{RNA}}\\
\frac{\mathrm{d}V_{\mathrm{mat}}}{\mathrm{d}t} &= k_{\mathrm{mat}}V_{g\mathrm{RNA}} - (k_{\rho_V} + d_{\mathrm{HIV}})V_{\mathrm{mat}}
\end{aligned}
\tag{3.1}
$$

where $[\mathrm{TR}] = [\mathrm{TR}_{\mathrm{cell}}] + f_{\mathrm{Tat}}\cdot[\mathrm{TR}_{\mathrm{Tat}}]$ is a transcription rate, and the effects of Tat and Rev are parameterized as $f_x = x/(1+x+K_xV_{\mathrm{int}}), x = \{\mathrm{Tat}, \mathrm{Rev}\}$. The effect of b_{ISG} on $V_{g\mathrm{RNA}}$ and V_{dsRNA} will be described below.

3.2. Antiviral IFN response

Intracellular IFN-I response against HIV consists of paracrine and autocrine signaling pathways. Autocrine pathway involves the recognition of viral RNA by the pattern recognition receptors and invoking IFN production. The result of this pathway is considered only for infected dendritic cell characterized by a constant IFN secretion rate, because in infected $\mathrm{CD4}^+$ T cells this pathway is largely suppressed

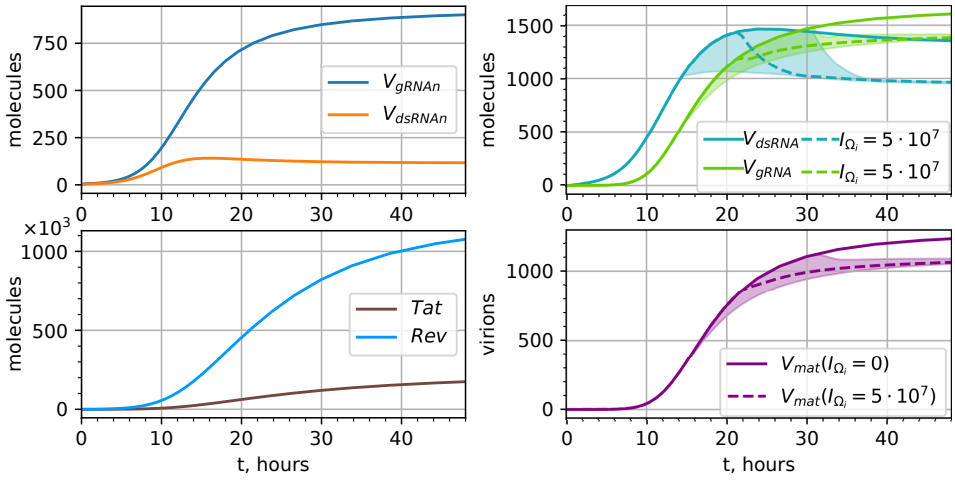

Figure 2. Intracellular HIV replication in productively infected cell with $V_{\text{int}} = 2$ integrated proviruses. Solid lines correspond to the absence of IFN response. The effect of IFN response on the number of viral RNA in cytoplasm $V_{\text{dsRNA}}, V_{g\text{RNA}}$ and mature virions V_{mat} is shown with dashed lines (medians) and uncertainty areas (interquartile ranges). Parameters of the model (rate constants are given in h^{-1} units): $d_{\text{HIV}} = 0.5, d_{DNA} = 0.2$, $[\text{TR}_{\text{cell}}] = 15$, $[\text{TR}_{\text{Tat}}] = 1500$, $K_{\text{Tat}} = 11000$ molecules, $K_{\text{Rev}} = 40000$ molecules, $k_{sp} = 2, \beta = 0.9, k_{\text{exp}} = 2.3, r_{\text{Tat}} = 6.55, r_{\text{Rev}} = 52.4, d_{\text{Tat}} = 0.04, d_{\text{Rev}} = 0.06, k_{\text{mat}} = 0.5, k_{\rho_V} = 0.15, r_{STAT} = 0.1, K_I = 1.23 \cdot 10^7$ molecules, $r_{\text{ISG}} = 0.1, k_{\text{ISG}} = 0.1$.

by HIV protease, Vif and Vpr proteins [20]. Paracrine signaling involves activation of STAT1/2 pathway (modelled as binary variable b_{ST}) by extracellular IFN-β I_{Ω_i}, that leads to expression of interferon stimulated genes (ISGs) (modelled as binary variable b_{ISG}), which increase degradation rates of HIV RNA in cytoplasm $V_{g\text{RNA}}$ and V_{dsRNA} (see (3.1)). The stochastic model of paracrine antiviral IFN response in infected T cells is based on work [16]. We consider the following cell states and transitions between states:

$$\{b_{ST} = b_{\text{ISG}} = 0\} \xrightarrow{a_{STAT}} \{b_{ST} = 1, b_{\text{ISG}} = 0\} \xrightarrow{r_{\text{ISG}}} \{b_{ST} = 1, b_{\text{ISG}} = 1\}$$

where $a_{STAT}(t) = r_{STAT} I_{\Omega_i}(t)/(K_I + I_{\Omega_i}(t))$ and r_{ISG} are propensity rates of transitions, $I_{\Omega_i}(t) = \int_{\Omega_i} I(\mathbf{x}, t)\mathrm{d}\mathbf{x}$. The reverse transitions are considered to be negligible for 48h-long simulations [16]. The resulting stochastic processes with time-dependent rates are simulated using temporal Gillespie algorithm as described in Subsection 2.2. The intracellular dynamics of HIV replication and the effect of antiviral IFN response in an infected cell harboring $V_{\text{int}} = 2$ genomes is presented in Fig. 2.

4. Numerical simulations of HIV infection dynamics in LN

In this section we describe some details of the implementation of the multiscale model. The following T cell subtypes are considered: CD4^+ T cells (infected and uninfected), CD8^+ T cells (nonspecific and HIV-specific effector cells, i.e., CTLs). We initialize the random spacial configuration of 1257 CD4^+ T cells, 3232 CD8^+

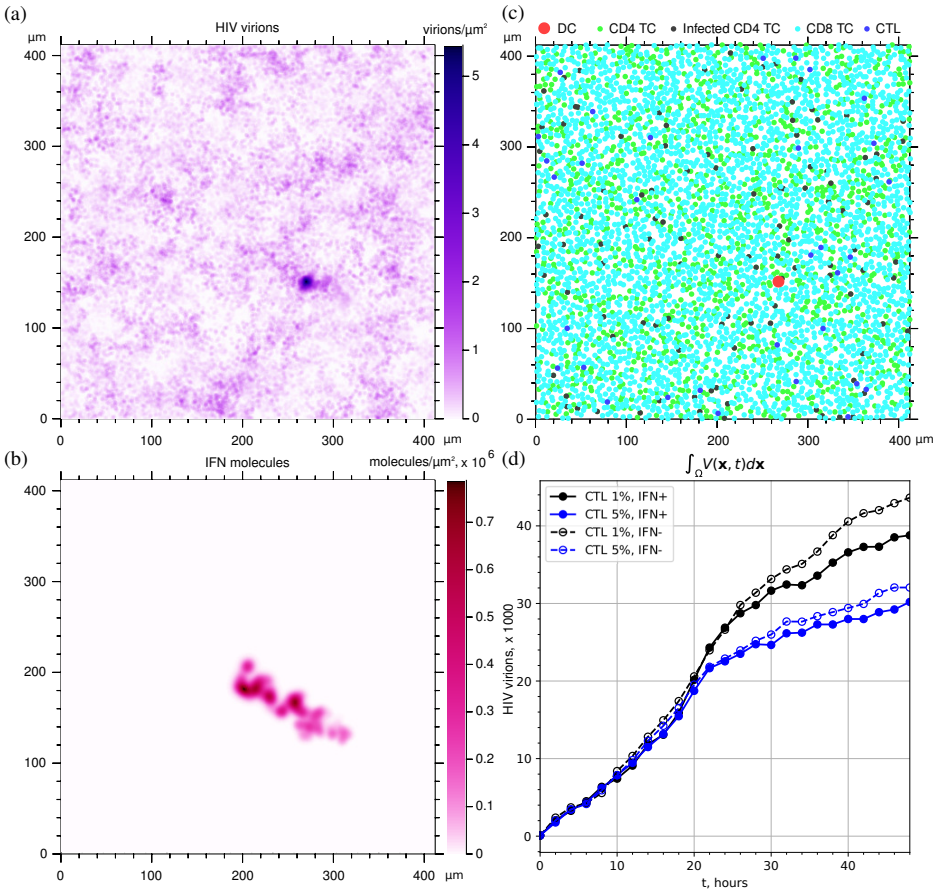

Figure 3. The local dynamics of HIV transmission in lymphoid tissue by one productively infected dendritic cell. (a)–(c) An example of extracellular fields of (a) HIV virions, (b) IFN molecules, and (c) spatial distribution of the immune cells (subtypes are indicated in color legend) 48 hours after infection of dendritic cell. (d) The dynamics of number of virions in the domain under normal conditions (black solid line), when CTL frequency is increased from 1% to 5% (blue lines), and when IFN response is switched off (dash lines). Lines correspond to median values of results of 3 numerical simulations.

T cells (32 of them are CTLs) in the domain Ω. The T cell lifespan is modelled as exponentially distributed with death rates $\gamma_{CD4} = 0.008$/day, $\gamma_{CD8} = 0.009$/day [2]. Infected CD4$^+$ T cells can be killed upon contact with HIV-specific CTLs. It is implemented by removing the infected cell after prolonged (>1min) contact or after multiple contacts with CTLs within 1 min. New T cells are introduced into the computational domain with rates $\lambda_{CD4} = 9$ cells/day, $\lambda_{CD8} = 30$ cells/day. When a new CD8$^+$ T cell is introduced, it is set to be a CTL with probability $p < f$, where $f = 0.01$ is the characteristic HIV-specific CTL frequency. If a newly placed cell overlaps with any other cell so that $h_{ij} < 5L/6$, then the placement attempt is rejected and the position of cell is resampled. We allow no more than 5 rejections. This procedure allows for nearly constant packing density of the domain and the long-

term homeostatic T cell subtype maintenance if there is no infection. We do not consider activation and division of cells in 48-hour simulations. To initiate local spread of infection, one productively infected dendritic cell is introduced into the domain and kept alive throughout the simulation. This dendritic cell secretes virions and IFN molecules with constant rates $k_{\rho_V}^{DC} = 500$ virions/h, $k_{\rho_I}^{DC} = 1.6 \cdot 10^4$ molecules/h [4], respectively, and participates in the cell-to-cell transmission of HIV. Virions are secreted by infected cells with the per cell rate $\rho_V^{(i)} = k_{\rho_V} V_{\text{mat}}^{(i)}$. Virions and molecules diffuse and degrade with the diffusion constants $D_V = 0.01, D_I = 0.34$ mm^2/h and decay rates $d_V = 0.5, d_I = 0.012$ h^{-1}, respectively (see [4, 16]).

Figure 3 illustrates the results of numerical simulation of the evolution of infection process over 48 hours. One can see extracellular fields of (a) HIV virions, (b) IFN molecules, and (c) the spatial distribution of cells (dendritic cell, infected and uninfected CD4$^+$ T cells, specific and nonspecific CD8$^+$ T cells) 48 hours postinfection. In Fig. 3d we present the dynamics of viral load, i.e., total number of virions in the whole domain Ω, in the absence of IFN response, for CTL frequency in LN ranging from 1% to 5%, and at combination of these perturbations.

5. Future work: multiscale modelling in 3D

In this study we developed the computational approach to mathematical modelling of immune processes in humans and animals following a multiscale hybrid framework. We presented the formulation and numerical implementation of multiscale mathematical model describing some of the key physical, biochemical, biological, and physiological processes which underlie the response of the immune system to HIV infection. Mathematically, the hybrid model is built by using various types and classes of equations, including ODEs, stochastic differential equations (SDEs), reaction–diffusion equations (RDEs), and Markov chain-based models (MCM). A computationally consistent and verified methodology for integration of various types of models representing specific modules of the immune system into global integrative models is elaborated. The following essential features constitute the core elements of our framework:

- for intracellular processes of immune cell fate regulation, both deterministic and related stochastic models are developed in pairs;
- the spatial population dynamics of immune cells and humoral factors in lymphoid organs is modelled with Newton's second law and reaction–diffusion equations, respectively, calibrated using experimental data for 2D consideration.

The existing studies in mathematical immunology on hybrid modelling are mostly restricted to the projection of immune processes on the 2D or 3D regular lattices which is a severe simplification of the physiology and anatomy of the immune system. The embedding of the multiscale models into the 3D spatially resolved geometrical model of LN is the direction of our future work.

References

1. J. Argilaguet, M. Pedragosa, A. Esteve-Codina, G. Riera, E. Vidal, C. Peligero-Cruz, V. Casella, D. Andreu, T. Kaisho, G. Bocharov, B. Ludewig, S. Heath, S. and A. Meyerhans, Systems analysis reveals complex biological processes during virus infection fate decisions. *Genome Research* **29** (2019), No. 6, 907–919.
2. G. Bocharov, V. Chereshnev, I. Gainova, S. Bazhan, B. Bachmetyev, J. Argilaguet, J. Martinez, and A. Meyerhans, Human immunodeficiency virus infection : from biological observations to mechanistic mathematical modelling. *Math. Model. Natur. Phenomena* **7** (2012), No. 5, 78–104.
3. A. Bouchnita, G. Bocharov, A. Meyerhans, and V. Volpert, Hybrid approach to model the spatial regulation of T cell responses. *BMC Immunology* **18** (2017), No. 1, 29.
4. A. Bouchnita, G. Bocharov, A. Meyerhans, and V. Volpert, Towards a multiscale model of acute HIV infection. *Computation* **5** (2017), No. 1, 6.
5. A. Cappuccio, P. Tieri, and F. Castiglione, Multiscale modelling in immunology: a review. *Briefings in Bioinformatics* **17** (2016), No. 3, 408–418.
6. N. A. Cilfone, D. E. Kirschner, and J. J. Linderman, Strategies for efficient numerical implementation of hybrid multi-scale agent-based models to describe biological systems. *Cellular and Molecular Bioengineering* **8** (2015), No. 1, 119–136.
7. N. M. Dixit and A. S. Perelson, Multiplicity of human immunodeficiency virus infections in lymphoid tissue. *J. Virology* **78** (2004), No. 16, 8942–8945.
8. R. N. Germain, M. Meier-Schellersheim, A. Nita-Lazar, and I. D. Fraser, Systems biology in immunology: A computational modelling perspective. *Annual Review of Immunology* **29** (2011), No. 1, 527–585.
9. S. Girel, C. Arpin, J. Marvel, O. Gandrillon, and F.Crauste, Model-based assessment of the role of uneven partitioning of molecular content on heterogeneity and regulation of differentiation in CD8 T-cell immune responses. *Frontiers in Immunology* **10** (2019), 230.
10. D. Grebennikov, A. Bouchnita, V. Volpert, N. Bessonov, A. Meyerhans, and G. Bocharov, Spatial lymphocyte dynamics in lymph nodes predicts the cytotoxic T cell frequency needed for HIV infection control. *Frontiers in Immunology* **10** (2019), 1213.
11. H. Kim and J. Yin, Robust growth of human immunodeficiency virus type 1 (HIV-1). *Biophysical J.* **89** (2005), No. 4, 2210–2221.
12. D. Kirschner, E. Pienaar, S. Marino, and J. J. Linderman, A review of computational and mathematical modelling contributions to our understanding of Mycobacterium tuberculosis within-host infection and treatment. *Current Opinion in Systems Biology* **3** (2017), 170–185.
13. W. Li, R. N. Germain, and M. Y. Gerner, High-dimensional cell-level analysis of tissues with Ce3D multiplex volume imaging. *Nature Protocols* **14** (2019), No. 6, 1708–1733.
14. V. M. Liarski, A. Sibley, N. van Panhuys, J. Ai, A. Chang, D. Kennedy, M. Merolle, R. N. Germain, M. L. Giger, and M. R. Clark, Quantifying in situ adaptive immune cell cognate interactions in humans. *Nature Immunology* **20** (2019), No. 4, 503–513.
15. B. Reddy and J. Yin, Quantitative intracellular kinetics of HIV type 1. *AIDS Research and Human Retroviruses* **15** (1999), No. 3, 273–283.
16. M. Rinas, Data-driven modelling of the dynamic competition between virus infection and the antiviral interferon response. *PhD Thesis*, University of Heidelberg, Heidelberg, 2015.
17. I. Sazonov, D. Grebennikov, M. Kelbert, and G. Bocharov, Modelling stochastic and deterministic behaviours in virus infection dynamics. *Math. Model. Natur. Phenomena* **12** (2017), No. 5, 63–77.
18. C. L. Sershen, S. J. Plimpton, and E. E. May, Oxygen modulates the effectiveness of granuloma

mediated host response to mycobacterium tuberculosis: A multiscale computational biology approach. *Frontiers in Cellular and Infection Microbiology* **6** (2016), 6.

19. A. Sigal, J. T. Kim, A. B. Balazs, E. Dekel, A. Mayo, R. Milo, and D. Baltimore, Cell-to-cell spread of HIV permits ongoing replication despite antiretroviral therapy. *Nature* **477** (2011), No. 7362, 95–98.

20. M. Solis, P. Nakhaei, M. Jalalirad, J. Lacoste, R. Douville, M. Arguello, T. Zhao, M. Laughrea, M. A. Wainberg, and J. Hiscott, RIG-I-mediated antiviral signaling is inhibited in HIV-1 infection by a protease-mediated sequestration of RIG-I. *J. Virology* **85** (2011), No. 3, 1224–1236.

21. C. L. Vestergaard and M. Génois, Temporal Gillespie algorithm: Fast simulation of contagion processes on time-varying networks. *PLOS Comput. Biology* **11** (2015), No. 10, e1004579.

22. C. Zhang, S. Zhou, E. Groppelli, P. Pellegrino, I. Williams, P. Borrow, B. M. Chain, and C. Jolly, Hybrid spreading mechanisms and T cell activation shape the dynamics of HIV-1 infection. *PLOS Comput. Biology* **11** (2015), No. 4, e1004179.